Climate
of the Past

Open Access

Eastern Mediterranean Sea circulation inferred from the conditions of S1 sapropel deposition

K. Tachikawa[1], L. Vidal[1], M. Cornuault[1], M. Garcia[1], A. Pothin[2], C. Sonzogni[1], E. Bard[1], G. Menot[1], and M. Revel[2]

[1]Aix-Marseille Université, CNRS, IRD, Collège de France, CEREGE UM34, 13545 Aix en Provence, France
[2]Geoazur, UMR 7329, 06560 Valbonne-Sophia Antipolis, France

Correspondence to: K. Tachikawa (kazuyo@cerege.fr)

Abstract. Holocene eastern Mediterranean Sea sediments contain an organic-rich sapropel S1 layer that was formed in oxygen-depleted waters. The spatial distribution of this layer revealed that during S1 deposition, deep waters were anoxic below a depth of 1800 m. However, whether this boundary permanently existed from the early to the mid-Holocene has not been examined yet. To answer this question, a multi-proxy approach was applied to a core retrieved close to the 1800 m boundary (at 1780 m). We measured the bulk sediment elemental composition, the stable isotopic composition of the planktonic foraminifer *Globigerinoides ruber* and the abundance of benthic foraminifera since the last deglaciation. The result indicates that authigenic U and Mo accumulation began around 13–12 cal ka BP, in concert with surface water freshening estimated from the *G. ruber* δ^{18}O record. The onset of bottom and pore water oxygen depletion occurred prior to S1 deposition inferred from barium enrichment. In the middle of the S1 deposition period, reduced authigenic V, Fe and As contents and the Br / Cl ratio indicated short-term bottom-water re-oxygenation. A sharp Mn peak and maximal abundance for benthic foraminifera marked a total recovery for circulation at approximately 7 cal ka BP. Based on our results and existing data, we suggest that S1 formation within the upper 1780 m of the eastern Mediterranean Sea was pre-conditioned by reduced ventilation, resulting from excess freshwater inputs due to insolation changes under deglacial conditions that initiated between 15 and 12 cal ka BP within the upper 1780 m. Short-term re-oxygenation in the Levantine Basin is estimated to have affected bottom water at least as deep as 1780 m in response to cooling and/or the reduction of freshwater inputs. We tentatively propose that complete ventilation recovery at the S1 termination was depth-dependent, with earlier oxygenation within the upper 1780 m. Our results provide new constraints on vertical water column structure in the eastern Mediterranean Sea since the last deglaciation.

1 Introduction

The Mediterranean Sea is located in a transition zone between subpolar depression and subtropical high pressure and is known to be sensitive to ongoing and past climate change (Bethoux and Gentili, 1999; Roether et al., 1996). Holocene sediments obtained from the eastern Mediterranean Sea often contain the most recent organic-rich sapropel deposit, S1 (10.8±0.4 to 6.1±0.5 cal ka BP; De Lange et al., 2008), that formed due to a drastic decrease in labile organic-matter decomposition (Moodley et al., 2005). Reduced oxygen supply to bottom waters has been suggested to be a precondition for sapropel formation although increased biological productivity further promoted S1 deposition (Bianchi et al., 2006; Myers et al., 1998; Rohling, 1994; Stratford et al., 2000).

Surface water density decreases due to excess freshwater inputs have played a pivotal role in reducing Mediterranean Sea thermohaline circulation during sapropel formation (Myers et al., 1998; Rohling, 1994; Stratford et al., 2000). By reinforcing Nile River discharge toward the Levantine Sea (Emeis et al., 2003; Kallel et al., 1997; Revel et al., 2010; Rohling, 1994; Rossignol-Strick et al., 1982), high summer insolation at minimum precession is known to have had a fundamental impact (Kutzbach et al., 2014; Rohling, 1994, and references therein; Ziegler et al., 2010). In parallel, due to an active Mediterranean storm track, reduced boreal win-

ter insolation could have favored winter precipitation over the Mediterranean Sea region (Kutzbach et al., 2014; Magny et al., 2013; Meijer and Tuenter, 2007; Rohling, 1994). The influence of a third freshwater source, Black Sea outflow, has been estimated to be minor, since the time of the Black and Mediterranean Sea connection (9–8 cal ka BP; Soulet et al., 2011; Vidal et al., 2010) was later than the onset of S1 deposition. Deglacial conditions were not compulsory for sapropel deposition (Rohling, 1994), even if sea-level rise and the consequent incursion of deglacial fresh Atlantic water towards the eastern Mediterranean Sea have possibly contributed to a surface water density decrease from 14.5 cal ka BP (Rohling et al., 2015).

In addition to orbitally driven insolation changes in a precession cycle, Mediterranean Sea bottom-water oxygenation records indicate centennial to millennial variability (Abu-Zied et al., 2008; Casford et al., 2003; De Rijk et al., 1999; Hennekam et al., 2014; Kuhnt et al., 2007; Rohling et al., 1997; Schmiedl et al., 2010). One of the most prominent changes occurred around 8 cal ka BP, mainly affecting shallow water masses (Rohling et al., 2015) at water depths of ≤ 1500 m in the southern Aegean Sea (example sites SL123 and LC-21, Fig. 1a and b) and ≤ 1200 m in the Adriatic Sea (example site MD90-917, not shown in figure; Siani et al., 2013). Both internal processes, such as winter cooling in the northern high latitudes (Schmiedl et al., 2010), and solar activity (Hennekam et al., 2014; Rohling et al., 2002) have been proposed to produce centennial to millennial variability in the eastern Mediterranean Sea.

The spatiotemporal distribution of S1 deposition in the eastern Mediterranean Sea could provide further insight into the water column structure during the Holocene. A compilation study revealed the presence of an anoxic boundary at a depth of about 1800 m (De Lange et al., 2008). However, the stability of this boundary from the early to the mid-Holocene is poorly known. Regional-scale modeling studies allowed an examination of the physical and biogeochemical processes behind S1 formation (Adloff, 2011; Adloff et al., 2011; Bianchi et al., 2006; Grimm, 2012; Meijer and Tuenter, 2007), but proxy reconstructions that can be compared with simulations are still scarce for the Holocene. This is because, under low-oxygen conditions, conventional approaches, such as benthic foraminiferal $\delta^{13}C$ measurements, suffer from epibenthic foraminifera paucity (Jorissen, 1999). Bulk sediment geochemistry provides complementary information when post-depositional elemental redistribution is carefully considered (Calvert and Fontugne, 2001; Reitz et al., 2006; Thomson et al., 1995, 1999; van Santvoort et al., 1996).

In this study, we investigated bottom-water oxygenation conditions using core MD04-2722 (33°06′ N, 33°30′ E, 1780 m water depth; Fig. 1) to analyze major, minor and trace elemental concentrations within bulk sediments obtained from XRF (X-ray fluorescence) scanning and ICP-MS (inductively coupled plasma spectrometry) measure-
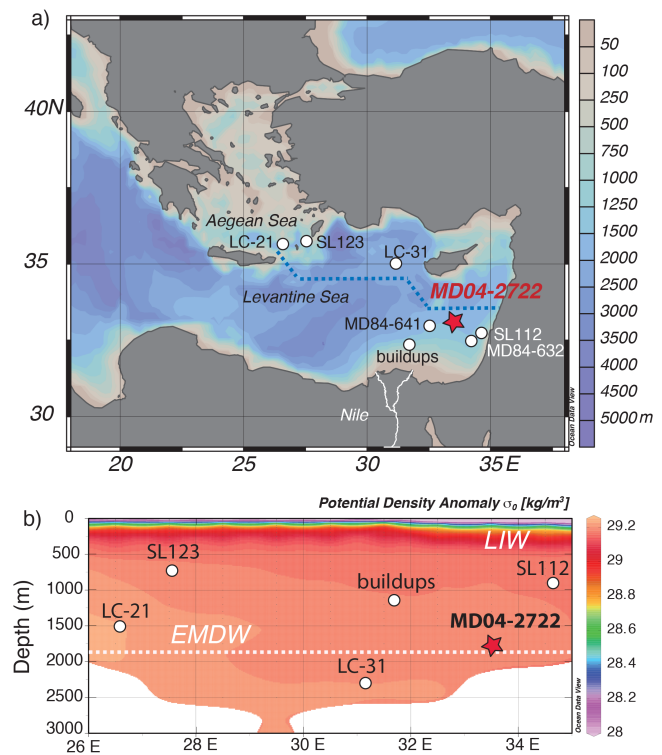
Figure 1. The core location map. **(a)** The core MD04-2722 (33°06′ N, 33°30′ E, 1780 m water depth) location on the bathymetry map. Site locations of the records discussed in the text are as follows: MD84-632: 32°28.2′ N, 34°13.2′ E (Essallami et al., 2007); MD84-641: 33°02′ N; 32°28′ E (Fontugne and Calvert, 1992); SL123: 35°45.3′ N, 27°33.3′ E (728 m water depth); SL112: 32°44.5′ N, 34°39.0′ E (892 m water depth) (Kuhnt et al., 2007); LC-21: 35°39.7′ N, 26°35.0′ E (1520 m water depth); LC-31: 34°59.8′ N, 31°09.8′ E (2300 m water depth) (Schmiedl et al., 2010); "buildups": 32°22′ N, 31°42′ E (1160 m water depth) (Bayon et al., 2013). **(b)** The present-day density anomaly transect along the dashed blue line at 34.5–35.5° N in Fig. 1a. The seawater temperature and salinity are from WOA09 (World Ocean Atlas 2009) (Antonov et al., 2010; Locarnini et al., 2010). The dashed white line indicates the upper limit of the permanent anoxic layer during S1 deposition at 1800 m (see the text for detail). Figures were generated using the Ocean Data View software (Schlitzer, 2009).

ments. Stable isotopic analyses of the surface-dwelling planktonic foraminifer *Globigerinoides ruber* (white) and benthic foraminiferal abundance were also conducted. Based on 12 ^{14}C dates of *G. ruber*, we established well-dated high-resolution records to provide a bottom-water ventilation history for the deep eastern Mediterranean Sea associated with S1 deposition.

2 Modern Mediterranean circulation and the study area

Present-day Mediterranean Sea thermohaline circulation is characterized by an anti-estuary pattern (Tomczak and God-

frey, 1994). Atlantic surface water enters the surface western and eastern Mediterranean Sea by passing through the Gibraltar and Siculo–Tunisian Straits, respectively. Through excess evaporation, the salinity of surface water continues to increase, forming Modified Atlantic Water (MAW). In the Levantine Sea (Fig. 1a), MAW flows along the African coast off the Nile River, then around Cyprus (Pinardi and Masetti, 2000). Between Cyprus and Rhodes, MAW is cooled by cold winter winds and can be transformed into Levantine Intermediate Water (LIW, 14 °C, salinity of 38.7, with a potential density anomaly $\sigma_o = 29.05$ kg m^{-3}; Fig. 1b) (Tomczak and Godfrey, 1994). The water mass occupies the depth of 200–500 m in the Levantine Sea and consists of the major water mass flowing back toward the western Mediterranean Sea through the Siculo–Tunisian Strait (Tomczak and Godfrey, 1994). Deep water found in the eastern Mediterranean Sea is an admixture consisting of LIW and Adriatic Sea surface water cooled by winter Bora winds (Tomczak and Godfrey, 1994). This Eastern Mediterranean Deep Water (EMDW; 13 °C, salinity of 38.6, $\sigma_o = 29.19$ kg m^{-3}; Fig. 1b) is less saline but colder and denser than LIW, located below 600 m in the eastern basin (Tomczak and Godfrey, 1994). In addition to the Adriatic Sea, deepwater formation was observed in the Aegean Sea in the 90s due to increased salinity (Roether et al., 1996). Activity in the zone as the site of deepwater formation is poorly known for the Holocene.

At the location of core MD04-2722, surface water corresponds to the MAW and the bottom-water mass is estimated to be EMDW (Fig. 1b).

3 Materials and methods

3.1 Materials

Core MD04-2722 (33°06′ N, 33°30′ E, 1780 m water depth, total core length of 36.96 m) was collected in the south of Cyprus in the eastern Levantine Sea (Fig. 1a) during the VANIL (Transit Valorisé Nil) cruise (R/V *Marion Dufresne*) conducted in 2004. In this study, we investigated the first 2.5 m of sediments that covers the past 23.6 cal ka BP (Sect. 4). The sediment is composed of a mixture of biogenic and fine terrigenous fractions (E. Ducassou, personal communication, 2014). The first 48 cm of the sediments is homogeneous and presents bioturbated hemipelagic mud facies. In the 48–62 cm interval, the core is brown with typical oxidized sediments. The boundary surrounding 62 cm is not completely horizontal due to sediment heterogeneity and/or coring processes. From 62 to 118 cm, sediments are dark green with an oily aspect and do not contain visible laminations. The interval from 118 to 250 cm consists of bioturbated hemipelagic mud facies. The color of sediments is represented in grayscale values (Fig. 2).

The core was sampled at every 2 cm interval for *G. ruber* (white) for stable isotope analysis. Benthic foraminiferal abundance was studied at a 2 cm interval for the first 134 cm
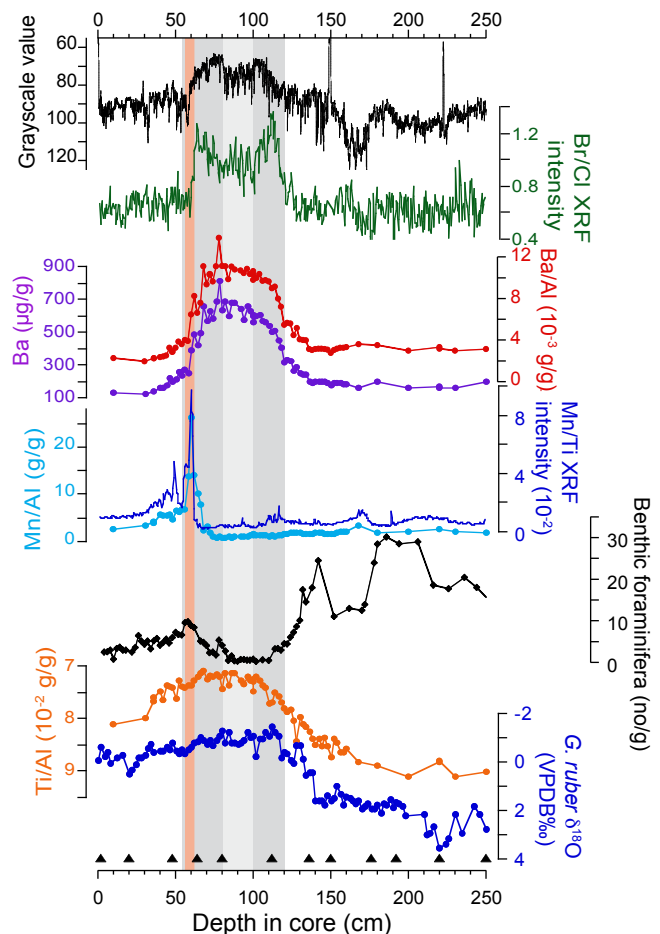
Figure 2. Characterization of the S1 interval recorded in core MD04-2722. Grayscale value, bulk elemental composition, benthic foraminiferal abundance (number of tests per unit of weight for dry bulk sediment), *G. ruber* δ^{18}O as a function of depth in core (cm). The S1 layer (55–120 cm) is shown with a dark grey band, the interval of low grayscale values (80–100 cm) with a light grey band and the interval of Mn enrichment (56–60 cm) with an orange band. Triangles indicate the depth levels dated by AMS (accelerator mass spectrometry) ^{14}C (see Table 1 for details).

and with 2–10 cm resolution for the deeper part. XRF scanning was performed every 5 mm over the depths studied. The bulk sediment elemental composition was determined at a 2 cm interval for 40–160 cm and at a 4–20 cm interval for other depth ranges.

3.2 Analytical methods

All analyses were performed at CEREGE (Centre Européen de Recherche et d'Enseignement de Géosciences de l'Environnement). High-resolution, non-destructive elemental analyses were performed using an XRF core scanner (ITRAX, Cox Analytical Systems). The relative abundance of S, Cl, Fe, Ti, V, Ca, Mn and Br was measured under different conditions. For Mn, V and Br measurements, a Mo tube

was used as the X-ray source at 30 kV and 40 mA with 20 s of counting. For other elements, a Cr tube was used at 30 kV and 30 mA with 20 s of counting. From the high-resolution optical image obtained by ITRAX, a grayscale profile was extracted using ImageJ software (http://imagej.nih.gov/ij/).

To determine the concentrations of Al, Ca, Ti, Fe, Mn, Ba, Mo, U, V, As, Sb, Ni, Co, Cu and Li in bulk sediments, well-homogenized, freeze-dried sediments (30 mg) were totally dissolved in a mixture of ultrapure acids (1.7 mL of 15 M HNO_3, 1.3 mL of 22 M HF and 0.1 mL of $HClO_4$). Obtained solutions were diluted and analyzed by an ICP-MS (Agilent 7500ce). The accuracy of measurements was estimated using analyses of geostandards MAG-1 (marine mud) and GSD12 (river sediment) that were subjected to the same digestion protocol as samples. The analytical uncertainty was less than 5 %, and blank levels for the digestion procedure were lower than 2 % of the mean measured concentration for all of the analyzed elements.

Calcite tests of *G. ruber* (white) were picked from the 250–355 μm size fraction. Foraminiferal $\delta^{18}O$ and $\delta^{13}C$ measurements were performed on a mass spectrometer (Finnigan Delta Advantage) equipped with a carbonate device. The measured isotopic values were normalized against the reference material NBS19. Mean external reproducibility was better than 0.05 ‰.

Benthic foraminifera abundance was determined by counting all existing calcareous specimens in the > 150 μm size fraction and dividing the number by the corresponding dry bulk sediment weight. Since the benthic foraminiferal abundance became very high in sediments below 134 cm, total benthic foraminiferal numbers were only counted for the first 132 cm. Dominant benthic foraminiferal species were identified for the studied interval.

4 Chronology

The chronology of core MD04-2722 is based on 12 AMS ^{14}C ages performed at the ARTEMIS (Accélérateur pour la Recherche en sciences de la Terre, Environnement, Muséologie, Implanté à Saclay) facility (Gif-sur-Yvette, France) on *G. ruber* (white) obtained from the > 150 μm size fraction. Conventional radiocarbon ages were converted into calendar ages based on MARINE13 (Reimer et al., 2013) using the ^{14}C calibration software CALIB 7.0.1 (Stuiver and Reimer, 1986–2013) (Table 1). The calibration integrates a marine ^{14}C reservoir age of 400 years that agrees well with the Mediterranean Sea surface water radiocarbon reservoir age of 390±85 years (Siani et al., 2000, 2001).

The estimated mean sedimentation rate was 12 cm kyr^{-1}. According to the age model, the typical temporal resolution for XRF measurements (5 mm), stable isotopes (2 cm) and ICP-MS measurements (2–10 cm) is approximately 40, 170 and 170–800 years, respectively.

Table 1. Radiocarbon ages for core MD04-2722.

Depth in core (cm)	AMS sample no.	^{14}C age ±1σ (yr BP)	Cal. age* (yr BP)	95.4 % (2σ) cal age ranges (yr BP)
2	SacA26352	3765±30	3700	3604–3812
20	SacA26353	4400±30	4551	4433–4678
48	SacA31590	5760±40	6188	6061–6277
64	SacA26354	6790±30	7318	7249–7396
80	SacA31591	7485±45	7945	7835–8042
112	SacA26355	8980±35	9629	9525–9763
136	SacA26356	10 680±40	12 048	11843–12292
150	SacA26357	11 925±40	13 377	13275–13483
176	SacA26358	13 675±45	15 955	15762–16130
192	SacA26359	15 170±50	17 964	17793–18139
220	SacA26360	18 030±60	21 313	21040–21555
250	SacA26361	20 000±70	23 611	23354–23878

* Median probability.

5 Results

For the interval studied, the Al and Ca concentrations in bulk sediments ranged between 4.4 and 6.9 % and between 10 and 17 %, respectively (not shown in the figure). Based on the assumption that the Al concentration in the detrital fraction was 8.0 % (upper continental crust; McLennan, 2001) and that all Ca was in the form of $CaCO_3$, we roughly estimated that the two major components in the bulk sediments were detrital (55–86 %) and carbonate (25–42 %) fractions. Considering the high proportion of the detrital component, enrichment of the analyzed elements was evaluated using normalization against Al. By taking into account the difficulty of precisely analyzing Al due to the attenuation of the XRF signal by pore water (Tjallingii et al., 2007), a Ti normalization was used for the XRF results.

5.1 Evaluation of the S1 layer

In core MD04-2722, the preserved S1 layer was visually recognized as the dark color between 60 and 120 cm, with the slightly lighter color interval from 80 to 100 cm shown in the grayscale profile (Fig. 2). High-resolution variability in organic-matter content was shown by a Br / Cl ratio profile obtained from an XRF scan (Fig. 2). Although Br XRF intensity and the Br / Cl ratio presented very similar variability (not shown in the figure), we used the Br / Cl XRF intensity ratio to better illustrate changes in the organic-matter content (Cartapanis et al., 2014) since Br is incorporated in marine organic matter but also exists in pore water (Cartapanis et al., 2011; Ziegler et al., 2008). High Br / Cl ratio values were found in the 55–120 cm interval, and a clear decrease existed between 60 and 110 cm (Fig. 2). Below 120 cm, the Br / Cl ratio was low and comparable to the core-top value (Fig. 2).

Barium enrichment has often been used to localize initial sapropel layers, since it is associated with biogenic barite ($BaSO_4$) that is an export production proxy resis-

tant to post-depositional oxidation (Calvert and Fontugne, 2001; De Lange et al., 2008; Thomson et al., 1995, 1999; van Santvoort et al., 1996). Both the Ba concentration and the Ba/Al ratio in core MD04-2722 displayed a similar convex-shaped peak from 55 to 120 cm, consistent with the high Br / Cl ratio interval (Fig. 2). The depth range of high Ba and organic-matter content at 55–120 cm corresponded to 6.8–10.4 cal ka BP (Table 1). This time span is, in general, in agreement with the previously estimated S1 deposition period from 6.1 ± 0.5 to 10.8 ± 0.4 cal ka BP (De Lange et al., 2008).

Close to the upper end of the Ba / Al ratio peak, prominent Mn enrichment was found at 56–60 cm (6.8–7.0 cal ka BP) for both the Mn / Al and Mn / Ti ratio profiles (Fig. 2). The peak shape of Mn / Al and Mn / Ti ratios was slightly different around 62 cm, possibly due to different sampling resolutions (1 cm for the Mn / Al ratio and 5 mm for Mn / Ti ratio) and the irregular brown-colored boundary at approximately 62 cm (see Sect. 3.1). As the Mn peak is mainly associated with the precipitation of Mn oxides under improved oxygenation, it often marks the end of S1 (Reitz et al., 2006). Taken together, we defined the S1 layer of core MD04-2722 as being at 55–120 cm (the dark grey band in Fig. 2).

The number of benthic foraminifera gradually increased from the core top to 56 cm and reached a maximum value at 56–58 cm with the Mn peak (Fig. 2). Between 55 and 142 cm, benthic foraminiferal abundance displayed a concave shape (Fig. 2). In the S1 layer, the sediment was void of benthic foraminifera at 104 cm (9.2 cal ka BP) and 108 cm (9.4 cal ka BP). Below 142 cm (12.6 cal ka BP), benthic foraminiferal abundance was higher than for the upper part. Major species identified within the studied interval included *Gyroidina* spp., *Cibicidoides pachyderma*, *Hoeglundina elegans*, *Cibicidoides wuellerstorfi*, *Uvigerina* spp., *Bolivina spathulata* and *Globobulimina* spp. (not shown in the figure). The first appearance of *Globobulimina* spp., indicators of low-oxygen content (Jorissen et al., 1995), is at 138 cm (12.2 cal ka BP). A detailed faunal assemblage will be provided elsewhere.

5.2 Indicators of dry or wet conditions

The major detrital fraction in the study area originated from the Nile River particles and Saharan dust (Krom et al., 1999). Ti / Al values have been used as an indicator of the relative proportion of Nile River particles to Saharan dust (Wehausen and Brumsack, 2000; Ziegler et al., 2010). In general, due to greater inputs of Al-rich river particles as compared to the contribution of Ti-rich dust inputs (Wehausen and Brumsack, 2000; Ziegler et al., 2010), the Ti / Al ratios of sediments far from the coastal zones in the eastern Mediterranean Sea were lower under wet conditions. Ti / Al values in core MD04-2722 varied from 0.07 to 0.09 g g^{-1} for the upper 250 cm with lower values between 35 and 230 cm (5.4–22.1 cal ka BP) (Fig. 2).

In addition to Ti / Al ratios, *G. ruber* δ^{18}O values reflect wet or dry conditions and also cool or warm surface water temperatures and continental ice volume. The isotopic values of core MD04-2722 ranged between -1.4 and 3.5 ‰, with minimum and maximum values at 112 cm (9.6 cal ka BP) and 220 cm (21.3 cal ka BP), respectively (Fig. 2). The interval for low *G. ruber* δ^{18}O values roughly agreed with the low Ti / Al interval (Fig. 2).

5.3 Redox-sensitive elements

Due to pyrite formation under reducing conditions, the sulfur content of bulk sediments is high in sapropel layers (Passier et al., 1996; Rohling, 1994). Considering that sulfur also exists in pore water in the form of the sulfate ion, we used the S / Cl ratio in core MD04-2722 to extract a signal closely related to pyrite even if S XRF intensity and S / Cl presented virtually identical profiles (not shown in figure). S / Cl values in core MD04-2722 indicated variability similar to the Ba / Al ratio (Fig. 3) but enrichment below the S1 layer at 120–150 cm (the darkest grey band in Fig. 3). This enrichment can be explained by downward sulfidization (see Sect. 6.1). The downward sulfidization could account for high values for the S / Cl, Ni / Al, As / Al and Fe / Al ratios below the S1 layer (Fig. 3) since As and Ni (and also Co and Cu) are often adsorbed and/or incorporated into pyrite (Large et al., 2014).

In general, high sedimentary Ni, Co and Cu concentrations are produced by enhanced productivity via the transfer of these elements due to the organic-matter flux and fixation in sediments under reducing environments (Cartapanis et al., 2011; Nameroff et al., 2002). Ni / Al values in core MD04-2722 were higher inside and below the S1 layer (Fig. 3). The Co / Al and Cu / Al ratios indicated variability comparable to the Ni / Al ratio (not shown in the figure).

A remarkable feature of the As / Al and Fe / Al profiles was strong depletion centered at 82–84 cm (around 8 cal ka BP inside the light grey band in Fig. 3). Depletion was also observed for the V / Al profile with a wider depth range between 80 and 110 cm (7.9–9.5 cal ka BP) (Fig. 3).

The U, Mo and Sb content of core MD04-2722 indicated a clear peak centered at the interval of the high Ba / Al ratio, but a detailed structure was specific to each element (Fig. 3). The U / Al profile indicated a smooth convex shape between 60 and 148 cm (7.0–13.2 cal ka BP), with a small negative spike at 84 cm (8.2 cal ka BP, inside the light grey band in Fig. 3). The main peak for the Mo / Al and Sb / Al ratios ranged between 70 and 138 cm (7.6–12.2 cal ka BP.) and 50 and 138 cm (6.3–12.2 cal ka BP), respectively (Fig. 3). The Mo / Al and Sb / Al ratios indicated a sharp peak from 56 to 60 cm, where the benthic foraminiferal number (Fig. 2) and the Mn content were at a maximum (the orange band in Fig. 3). In addition to the Mo / Al and Sb / Al ratios, the Li / Al ratios of core MD04-2722 presented a peak synchronous with the high Mn content (Fig. 3).
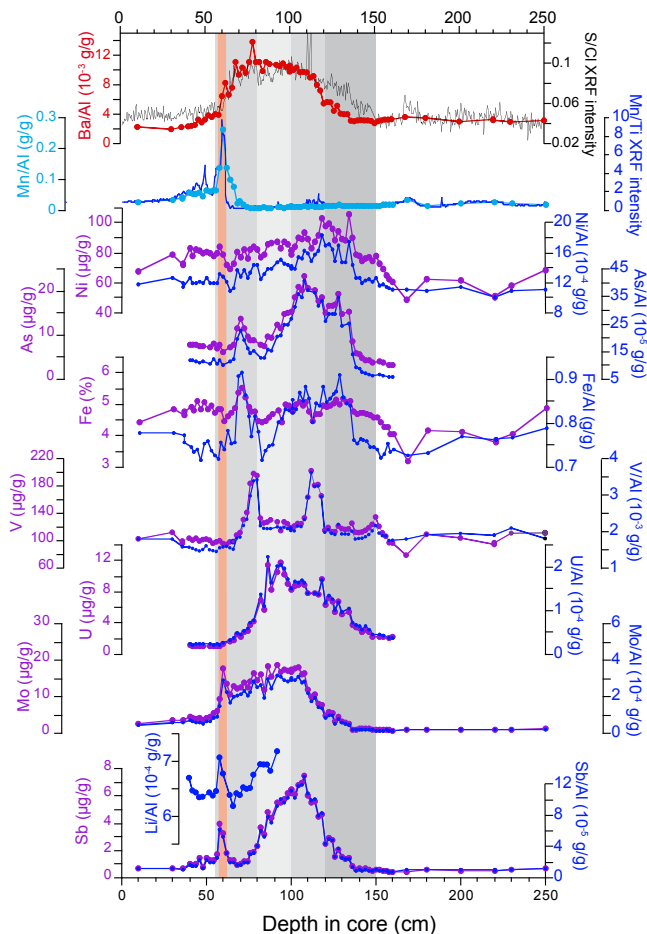
Figure 3. The elemental concentrations and the element / Al ratios for the bulk sediment of MD04-2722 as a function of depth in core, together with the S / Cl XRF intensity. Dark and light grey bands indicate the S1 layer determined from Ba enrichment (55–120 cm) and the interval of low grayscale values (80–100 cm), respectively. The darkest grey band and the orange band indicate the interval affected by downward sulfidization (Passier et al., 1996) (120–150 cm) and Mn enrichment (56–60 cm), respectively.

6   Discussion

Redox-sensitive elements and benthic foraminiferal abundance in core MD04-2722 can be used as an indicator of bottom or pore water conditions, which, in turn, are modulated by bottom-water ventilation and biological productivity, whereas the Ti / Al ratio and *G. ruber* δ^{18}O records reflect wet or dry conditions. In the following discussion, we first describe the geochemical meaning of the different elemental ratios that can be used to infer Mediterranean Sea ventilation. We then propose deepwater conditions for the onset, during and at the termination of S1 deposition by combining all of the data obtained.

6.1   Geochemical meaning of elemental ratios

During sapropel deposition, sulfate reduction occurred and HS^- excess for pyrite precipitation migrated downwards, whereas pore water Fe^{2+} existing below the sapropel layer moved upwards, leading to pyrite precipitation (Passier et al., 1996). The process is called downward sulfidization and impacts the distribution of trace elements such as Ni, Co, As and Cu associated with pyrite (Passier et al., 1996). Hence, the enrichment of Ni, Co and Cu below the S1 interval may not signify an increase in biological productivity prior to S1 deposition. Considering the difficulty in interpreting peaks below the S1 layer, here, we do not discuss them further.

Due to insoluble chemical speciation in reducing environments, authigenic U and Mo accumulate under suboxic and anoxic conditions, respectively (Algeo and Maynard, 2004; Klinkhammer and Palmer, 1991; Tribovillard et al., 2006). The accumulation of these elements does not necessarily indicate that the bottom water was permanently highly depleted in oxygen. Enrichment could reflect suboxic or anoxic pore water conditions related to slow ventilation and/or high organic rain. Taking this fact into account, we carefully evaluated potential circulation changes by combining the U / Al and Mo / Al profiles of core MD04-2722 (Fig. 3) with results from previous studies (see Sect. 6.2).

In the middle of the S1 unit, the sediment color was lighter and the sedimentary organic matter (Br / Cl ratio) and redox-sensitive element (Fe / Al, As / Al and V / Al ratios) were lower (light grey band in Figs. 2 and 3). The observed change could be explained by the injection of dissolved oxygen into the water column via re-ventilation. The oxidation of organic matter within the water column and on the sea floor can reduce sedimentary Br / Cl values. The pyrite in sediments can be oxidized to iron oxides and/or to hydroxides when it is in contact with dissolved oxygen (Chandra and Gerson, 2011). If these oxides and/or hydroxides are again reduced in sediments, Fe and As associated with pyrite would be released to pore water. Vanadium accumulation in anoxic sediments commonly takes place via diffusion across the sediment–water interface, and the release of this element occurs when Mn is reduced (Nameroff et al., 2002). We investigate this issue in Sect. 6.3.

The origin of the Mn peak at the end of S1 has been extensively discussed in previous studies (Reitz et al., 2006; Thomson et al., 1995, 1999; van Santvoort et al., 1996). Core MD04-2722 only contains one Mn peak at the end of the S1 unit (Fig. 2), and the Mo / Al, Sb / Al and Li / Al ratios synchronously increase with Mn (Fig. 3). Since Mo (Shimmield and Price, 1986; Tribovillard et al., 2006), As (Cutter et al., 2001, and references therein) and Li (Reitz et al., 2006) can be scavenged by Mn oxides, the peaks observed for core MD04-2722 were likely produced from water column oxygenation at the S1 termination (Sect. 6.4).

The following discussion focuses on the state of bottom-water circulation in the deep eastern Mediterranean Sea dur-

ing the following periods: (i) the onset of S1 deposition, (ii) oxygenation event(s) in the middle of the S1 unit and (iii) the termination of S1 deposition. We are aware that, due to diagenetic processes and post-depositional diffusion that can modify boundary positions, the precise timing of ventilation changes is difficult to obtain from a single-proxy profile. Considering the fact that the distribution of each element is determined by element-specific processes, we interpret and discuss the timing of ventilation changes when several proxy reconstructions indicate consistent changes.

6.2 Conditions of bottom-water circulation prior to S1 deposition

In core MD04-2722, U / Al and Mo / Al ratios began to increase from 13 cal ka BP (148 cm) to 12 cal ka BP (138 cm; Figs. 3 and 4). This time span also corresponds to the beginning of a decrease in the number of benthic foraminifera (12.2 cal ka BP, 138 cm; Figs. 2 and 4) that was high in well-oxygenated glacial bottom waters. Two major factors affecting benthic foraminiferal assemblage are food supply and water oxygenation (Jorissen et al., 1995). Since the Ba / Al change indicates an increasing trend of export production just before the S1 deposition (Fig. 2), it is logical to assume that the observed reduction in benthic foraminiferal number was related to oxygen depletion. Therefore, the result can be interpreted as meaning that the onset of oxygen depletion for bottom and/or pore waters at a depth of 1780 m started prior to S1 deposition. Since surface water freshening has been considered to be the main factor affecting Mediterranean Sea thermohaline circulation (De Lange et al., 2008; Emeis et al., 2000; Rohling, 1994), we examine the timing of the onset of wet conditions, changes in surface hydrology and deepwater circulation using records obtained from core MD04-2722.

Decreases in the Ti / Al ratio and *G. ruber* δ^{18}O in core MD04-2722 began prior to S1 deposition (Fig. 4). To better illustrate surface water salinity changes in the Levantine Sea, the *G. ruber* δ^{18}O record is combined with a sea surface temperature (SST) reconstruction that is based on planktonic foraminiferal assemblages obtained from a neighboring site (core MD84-632; 32°28′ N, 34°13′ E; Essallami et al., 2007; Fig. 1a). The present-day bottom-water δ^{18}O value (Pierre, 1999) is then subtracted so that the local δ^{18}O$_w$ anomaly can be calculated (Fig. 4). A marked decrease in the δ^{18}O$_w$ anomaly began at approximately 12 cal ka BP (Fig. 4). Variability mainly stems from the core MD04-2722 *G. ruber* δ^{18}O record, not from temperature, because the major feature is maintained when another SST record from a nearby site is applied (Castañeda et al., 2010). We note here that the large amplitude of the seawater δ^{18}O anomaly change of 2.7 ‰ from 20.1 to 9.6 cal ka BP cannot be explained by a global δ^{18}O change related to continental ice volume (Waelbroeck et al., 2002). Another record of *G. ruber* δ^{18}O from a nearby site (core MD84-641; 33°02′ N; 32°28′ E, 1375 m water depth) (Fontugne and Calvert, 1992) indicates a very
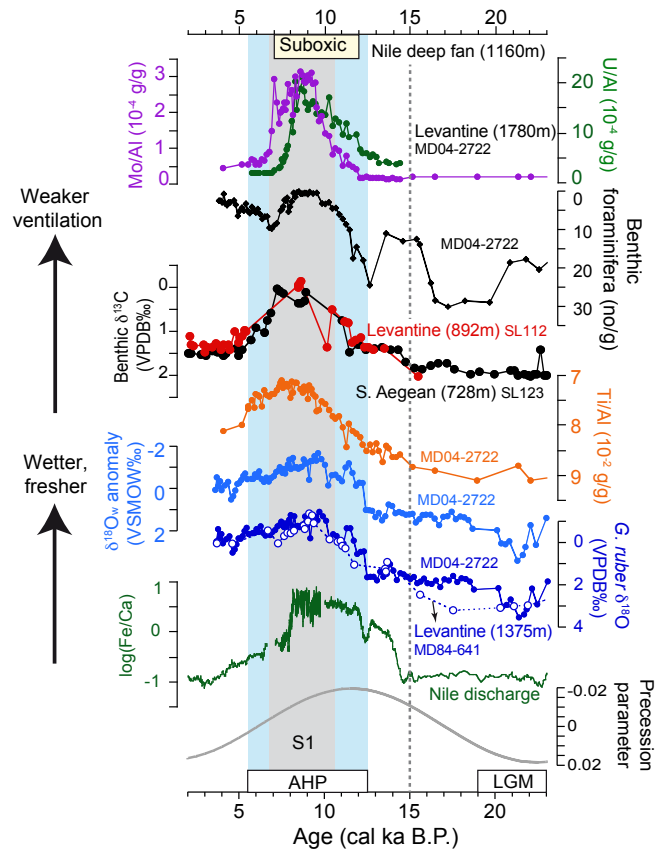
Figure 4. The last 23 kyr variability of proxies for ventilation (U / Al, Mo / Al and benthic foraminiferal density) and wet or fresh conditions (Ti / Al and seawater δ^{18}O anomaly) based on core MD04-2722 results as compared with previous studies. The surface water δ^{18}O anomaly was calculated by combining the *G. ruber* δ^{18}O record from core MD04-2722 with the SST reconstruction (see text for detail). Suboxic conditions on the Nile deep fan were estimated to have lasted from 12 to 7 cal ka BP at the "buildups"' location (Fig. 1a and b) (Bayon et al., 2013). Benthic foraminiferal δ^{13}C records were based on the epibenthic foraminifer species *Planulina ariminensis* (Kuhnt et al., 2007; Schmiedl et al., 2010). Changes in Nile River discharge are shown with the log scale Fe / Ca ratio for core MS27PT, located close to the Rosetta Mouth of the Nile River (Revel et al., 2014). The precession parameter is from Laskar et al. (2004). The blue zone indicates the African Humid Period (AHP, 12.5–5.5 cal ka BP) based on Adkins et al. (2006) and deMenocal et al. (2000). The grey band indicates the S1 period from 10.4 to 6.8 cal ka BP, estimated for core MD04-2722. The dashed line presents the possible onset for weaker ventilation at 15 cal ka BP in the eastern Mediterranean Sea. LGM: Last Glacial Maximum.

similar variability to the core MD04-2722 record, attesting that the *G. ruber* δ^{18}O variability represents regional hydrological changes.

The δ^{18}O$_w$ anomaly and Ti / Al records indicate the beginning of a fresher and wetter period at approximately 12 and 15 cal ka BP, respectively, comparable with the incep-

tion of the African Humid Period at 12.5 cal ka BP (Adkins et al., 2006; deMenocal et al., 2000) and increased Nile River discharge (Revel et al., 2014) in response to insolation changes (Laskar et al., 2004) (Fig. 4). Our result is consistent with the hypothesis that Nile River discharge was one of the main freshwater sources for the Levantine Sea (Rossignol-Strick et al., 1982). Indeed, the influence of Nile River discharge was estimated to have spread as far as Cyprus (Almogi-Labin et al., 2009) (Fig. 1a).

The spatial extension of weakly ventilated waters can be evaluated by comparing it to previously reported records from the eastern Mediterranean Sea. Based on the U–Th dating of authigenic carbonates formed in reducing environments, the start of suboxic bottom-water conditions was estimated to be 12 cal ka BP on the Nile River deep fan at a depth of 1160 m ("buildups"; Bayon et al., 2013) (Figs. 1a, b and 4). Based on decreasing benthic foraminiferal δ^{13}C values that began at 15 cal ka BP (Fig. 4), weaker ventilation has also been estimated for a water depth of approximately 700 m in the southern Aegean Sea (site SL123) and for a water depth of approximately 900 m in the southeast Levantine Sea (site SL112) (Kuhnt et al., 2007; Schmiedl et al., 2010) (Fig. 1a, b). It is worth noting that the decreasing trend of foraminiferal benthic δ^{13}C values does not necessarily a mean complete shutdown of ventilation. The δ^{13}C values (Fig. 4) were still comparable to the late Holocene values, and both benthic foraminiferal assemblage and trace elements (Fig. 5) did not indicate strong anoxic conditions before the S1 interval. We thus propose a reduced intermediate or deepwater formation and consequently a restricted extension of well-oxygenated water mass(es) for this period. Productivity change is estimated to have a second role because it would be more local or regional, reflecting coastlines, local nutrient supplies, such as riverine inputs, and the topography of lands that impact wind regimes.

The net increase in freshwater inputs reinforced vertical salinity gradients in the eastern Mediterranean Sea, which in turn shoaled the pycnocline at a depth shallower than the euphotic layer, allowing the development of a deep-chlorophyll maximum relative to the present day in the easternmost Mediterranean Sea (Castradori, 1993; Grelaud et al., 2012; Rohling, 1994). A shoaling pycnocline and a greater nutrient supply due to Nile River discharge (Herut et al., 2000) could have contributed to enhanced biological productivity. Considering the time required for circulation reorganization, the gradual consumption of existing dissolved oxygen in the water column by organic decomposition and the improvement of sedimentary organic-matter preservation under oxygen-depleted conditions (Hartnett et al., 1998), it is not surprising that a net increase in the Br / Cl ratio in core MD04-2722 appeared later than the onset of slow bottom-water circulation (Figs. 2 and 3).

Recent regional-scale modeling studies have proposed that initial glacial conditions were a key parameter for forming S1 deposition (Adloff, 2011; Grimm, 2012). Sen-
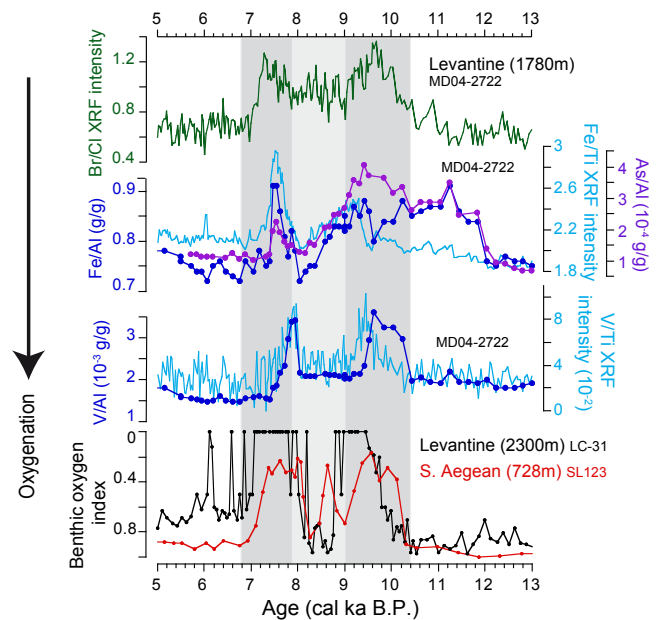
Figure 5. Re-oxygenation in the middle of the S1 interval as inferred from the bulk geochemistry (Br / Cl, Fe / Al, Fe / Ti, As / Al, V / Al and V / Ti ratios) in core MD04-2722 and the benthic foraminiferal oxygen index obtained at sites LC-31 and SL123 (Schmiedl et al., 2010) (Fig. 1a, b). Dark and light grey bands indicate the S1 unit (10.4–6.8 cal ka BP) and the interval of low grayscale values (9.0–7.9 cal ka BP) in core MD04-2722, respectively.

sitivity experiments indicate that freshwater contributions and increased productivity are not sufficient for attaining the observed bottom-water oxygen depletion (Adloff, 2011; Grimm, 2012). Only a simulation that considered initial glacial conditions succeeded in maintaining oxygen depletion for several thousand years, comparable to S1 duration (Grimm, 2012). The inception of weaker ventilation during the glacial–interglacial transition, as proposed in this study, is in line with these recent simulations.

6.3 Re-ventilation in the middle of the S1 period

The lighter color of the sediment and the clear decrease in the Br / Cl (Fig. 2), As / Al, Fe / Al and V / Al ratios (Fig. 3) in core MD04-2722 indicate temporally improved oxygenation in the water column and in pore water in the middle of the S1 period. Since the Ba / Al ratio did not show clear diminution at this interval (Fig. 2), biological productivity was not responsible for the change. Improved oxygenation seems to be related to an active re-ventilation that promoted organic-matter degradation in the water column and post-depositional oxidation (Thomson et al., 1999). To examine the variability in detail, we combine highly resolved Br / Cl, Fe / Ti and V / Ti records with Fe / Al, As / Al and V / Al ratios (Fig. 5). The major decline in the Fe / Al, Fe / Ti and

As / Al ratios is centered at 8.4–8.2 cal ka BP, whereas minimal Br / Cl, V / Al and V / Ti ratios extended between 9.5 and 7.9 ca ka BP (Fig. 5). A longer depletion period for the Br / Cl, V / Al and V / Ti ratios can be explained by continuous organic-matter oxidation, with oxygen penetrating into sediments as well as the subsequent reduction of Mn oxides (see Sect. 6.1).

Our results indicate that re-ventilation event(s) affected bottom water located at the upper limit of the anoxic layer at 1800 m (De Lange et al., 2008). By combining the results of core MD04-2722 with previously reported high-resolution records, we examine the spatial coverage of re-oxygenation. In addition to shallow Adriatic Sea (MD90-917; 41°17′ N, 17°37′ E, 1010 m, not shown in the figure; Siani et al., 2013) and shallow southern Aegean Sea (sites LC-21 and SL123 ≤ 1500 m; Fig. 1), benthic foraminiferal assemblage indicates re-ventilation in the Levantine Sea at water depths ranging from 900 m (site SL112, Fig. 1; Schmiedl et al., 2010) to 2300 m (site LC-31, Fig. 1; Abu-Zied et al., 2008; Schmiedl et al., 2010). We propose two hypotheses about re-ventilation depths. Firstly, the re-ventilation affected the water column down to 2300 m. The second possibility is that the re-ventilation was limited to water depths shallower than 1800 m, taking into account the fact that core LC-31 contains a small slump confirmed by AMS ^{14}C dates inside of the S1 layer (Abu-Zied et al., 2008). In any case, the large spatial distribution of the S1 interruption at least as deep as 1780 m suggests a basin-wide reorganization for ventilation.

Cores presenting the S1 interruption are currently bathed in well-oxygenated EMDW (Figs. 1b and 5). At present, the formation of EMDW is controlled by the winter cooling of surface water in the Adriatic Sea and occasionally in the Aegean Sea (Roether et al., 1996), as well as by the salinity of LIW (Sect. 2). Holocene surface water winter cooling in the Aegean Sea has been demonstrated to occur with atmospheric circulation changes in relation to the winter and spring Siberian High at 9.5–9.1 and 8.8–7.8 cal ka BP (Kotthoff et al., 2008; Marino et al., 2009; Mayewski et al., 1997) and for the 8.2 cal ka BP event (Pross et al., 2009) recorded in Greenland ice cores (Alley and Ágústsdóttir, 2005). Due to the cold air flux from polar regions, surface water in convection zones could be cooled during winter, leading to the activation of deepwater formation in the Aegean (Schmiedl et al., 2010) and/or the Adriatic (Siani et al., 2013) seas. A numerical simulation has indicated that a surface eastern Mediterranean Sea cooling of 2–3 °C could trigger deep convection in the Adriatic Sea and intermediate-water formation in the Aegean Sea, leading to oxygenation for the upper 1250 m water masses of the eastern Mediterranean Sea (Myers and Rohling, 2000)

On the other hand, reconstructed Nile River discharge (Fig. 4) presented a high-frequency variability and a decline around 8 cal ka BP (Blanchet et al., 2014; Revel et al., 2014). Planktonic foraminiferal Ba / Ca ratios indicate the fluctua-
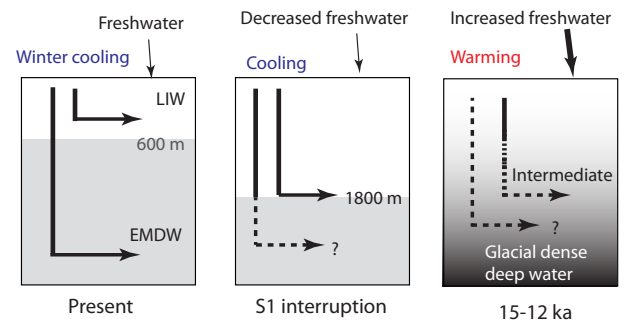
Figure 6. Schematic ventilation patterns in the eastern Mediterranean Sea at present, S1 interruption and 15–12 cal ka BP.

tion in Nile River discharge at 8.4–8.2 cal kyr BP (Weldeab et al., 2014). Reduced Nile River discharge could have led to a salinity rise for LIW that mixed with surface Adriatic Sea water, contributing to the activation of EMDW formation. Thus, both temperature and salinity effects could be factors for re-ventilation in the eastern Mediterranean Sea (Fig. 6) in relation to northern high-latitude and tropical or subtropical climate conditions.

During the interruption period, the vertical density gradient was attenuated, leading to partial mixing between old dense glacial waters and overlaying lighter waters. Once cooling and/or reduced freshwater input finished, the stagnant ventilation mode returned, which suggests that the density barrier was still too strong to shift to the present-day circulation mode. If the duration of cooling and less freshwater inputs, the size of this forcing, and the spatiotemporal S1 interruption are quantified, the interruption can provide information regarding the sensitivity of the eastern Mediterranean thermohaline circulation.

6.4 Total ventilation recovery at the S1 termination

Mn / Al, Mn / Ti, Mo / Al, Li / Al and Sb / Al ratios (Fig. 3), as well as the benthic foraminiferal abundance of core MD04-2722 (Fig. 2), indicated a synchronous increase at 7.0 cal ka BP (60 cm) to 6.8 cal ka BP (56 cm), suggesting oxygenation in the water column at the core location. The age range for the increase was slightly earlier than the basin-wide S1 termination of 6.1±0.5 cal ka BP that was estimated using the cores from water depths down to 3400 m (De Lange et al., 2008) although, considering the dating uncertainty, the difference was subtle. If the age difference is real, the S1 termination may be characterized by depth-dependant ventilation recovery with earlier oxygenation at depths shallower than 1800 m. Based on previous observations, we suggest this possibility. At first, benthic ecosystem recovery at the S1 termination was depth-dependent, with a prior recovery at shallower depths in the eastern Mediterranean Sea (Schmiedl et al., 2010). The second point is the possible existence of dense deep water. Modeling studies have indicated that the

deepwater mass was much denser than that of shallower waters because the latter contained saline glacial water (Grimm, 2012; Myers et al., 1998) (Fig. 6). If the increase in surface water density did not exceed the density of this dense water below, ventilation would affect only lighter water masses at shallower depths.

Ventilation recovery can be explained both by the reduction of riverine freshwater inputs and surface water cooling. A 9000-year-long transient model with insolation and atmospheric greenhouse gas forcing simulated a gradual precipitation decline over eastern Africa from the early to the late Holocene (Renssen et al., 2006). Reconstructed Nile River discharge (Blanchet et al., 2014; Revel et al., 2014; Weldeab et al., 2014) displayed a decreasing trend from the early to mid-Holocene (Fig. 4). Approximately 3 °C of the SST decrease during April–May was recorded in the southern Adriatic between 7.1 and 6.9 cal ka BP (Siani et al., 2013). In the southern Aegean Sea during winter, an approximate 2–3 °C in surface water cooling was observed from 7.5 to 7.0 cal ka BP (Marino et al., 2009). Once surface water density within the deep- and intermediate-water formation zones exceeded the threshold value, water convection could restart. The onset of these cooling records is consistent with our estimation for total ventilation recovery at water depths shallower than 1800 m from 7.0 to 6.8 cal ka BP.

Considering the subtle density difference between the present LIW and EMDW (Sect. 2) and distinct climate background between the present and the moment of S1 termination, it is impossible to precisely identify the physical mechanisms of total ventilation recovery. Nonetheless, if ventilation recovery was water-depth-dependent, the S1 termination contrasted with re-ventilation event(s) during the S1 period, affecting waters below the critical depth of 1800 m in the Levantine Sea (Figs. 5 and 6). The finding provides new constraints on vertical structure within the eastern Mediterranean Sea during S1 deposition.

7 Conclusions

We analyzed the bulk sediment elemental composition, the δ^{18}O of *Globigerinoides ruber* and the abundance of benthic foraminifera since the last deglaciation within core MD04-2722 obtained from the Levantine Sea. Water depth at the core location was close to the estimated anoxic-layer upper limit for the most recent sapropel S1 deposition (1800 m) and rendered the site highly sensitive to past circulation changes. By combining our new results with previous studies, some fundamental features for ventilation in the eastern Mediterranean Sea were identified.

Bulk sediment Ti / Al ratios and the surface water δ^{18}O anomaly calculated from the *G. ruber* δ^{18}O obtained from core MD04-2722 indicated that a wet period and fresher surface water appeared at the core site around 15–12 cal ka BP. The enrichment of Mo and U, as well as ben-

thic foraminiferal density, indicated that surface hydrological changes were transferred to bottom water, leading to the reduction of deep- and intermediate-water formation and the consequent restricted expansion of oxygenated water masses that began prior to S1 deposition. Our results are consistent with previous reconstructions and regional-scale simulations and support the idea that a reduced oxygen supply due to slow ventilation was a precondition of S1 formation.

Decreased Br / Cl, Fe / Al, Fe / Ti, V / Al, V / Ti and As / Al ratios indicated that temporal re-oxygenation event(s) occurred during the middle of the S1 period. Improved oxygenation was produced by active re-ventilation rather than reduced biological productivity and affected water depths at least as deep as 1800 m in the Levantine Basin. Winter cooling in the Aegean and Adriatic Seas in relation to northern high-latitude conditions and salinity increases related to reduced Nile River discharge contributed to the temporal reactivation of thermohaline circulation in the eastern Mediterranean Sea.

From the concomitant peak of Mn, Mo, Sb and Li and for the increased abundance of benthic foraminifera, a total recovery in ventilation at the core MD04-2722 site was estimated to have occurred at 7.0–6.8 cal ka BP. We tentatively propose a depth-dependent S1 termination with an earlier ventilation at water depths shallower than 1800 m. This study provides new constraints on the eastern Mediterranean Sea bottom-water circulation since the last deglaciation that could be examined by future modeling studies.

References

Abu-Zied, R. H., Rohling, E. J., Jorissen, F. J., Fontanier, C., Casford, J. S. L., and Cooke, S.: Benthic foraminiferal response to changes in bottom-water oxygenation and organic carbon flux in the eastern Mediterranean during LGM to recent times, Mar. Micropaleontol., 67, 46–68, 2008.

Adkins, J., deMenocal, P., and Eshel, G.: The "African humid period" and the record of marine upwelling from excess ^{230}Th in Ocean Drilling Program Hole 658C, Paleoceanography, 21, PA4203, doi:10.1029/2005PA001200, 2006.

Adloff, F.: Early Holocene Eastern Mediterranean Ocean Climate and the Stability of its Overturning Circulation, PhD thesis, International Max Planck Research School on Earth System Modelling, Max Planck Institute, Hamburg, Germany, 2011.

Adloff, F., Mikolajewicz, U., Kučera, M., Grimm, R., Maier-Reimer, E., Schmiedl, G., and Emeis, K.-C.: Corrigendum to "Upper ocean climate of the Eastern Mediterranean Sea during the Holocene Insolation Maximum – a model study" published in Clim. Past, 7, 1103–1122, 2011, Clim. Past, 7, 1149–1168, doi:10.5194/cp-7-1149-2011, 2011.

Algeo, T. J. and Maynard, J. B.: Trace-element behavior and redox facies in core shales of Upper Pennsylvanian Kansas-type cyclothems, Chem. Geol., 206, 289–318, 2004.

Alley, R. B. and Ágústsdóttir, A. M.: The 8k event: cause and consequences of a major Holocene abrupt climate change, Quaternary Sci. Rev., 24, 1123–1149, 2005.

Almogi-Labin, A., Bar-Matthews, M., Shriki, D., Kolosovsky, E., Paterne, M., Schilman, B., Ayalon, A., Aizenshtat, Z., and Matthews, A.: Climatic variability during the last ∼ 90 ka of the southern and northern Levantine Basin as evident from marine records and speleothems, Quaternary Sci. Rev., 28, 2882–2896, 2009.

Antonov, J. I., Seidov, D., Boyer, T. P., Locarnini, R. A., Mishonov, A. V., Garcia, H. E., Baranova, O. K., Zweng, M. M., and Johnson, D. R.: World Ocean Atlas 2009, Volume 2: Salinity, in: NOAA Atlas NESDIS 68, edited by: Levitus, S., U.S. Government Printing Office, Washington, D.C., 2010.

Bayon, G., Dupre, S., Ponzevera, E., Etoubleau, J., Cheron, S., Pierre, C., Mascle, J., Boetius, A., and de Lange, G. J.: Formation of carbonate chimneys in the Mediterranean Sea linked to deep-water oxygen depletion, Nat. Geosci., 6, 755–760, 2013.

Bethoux, J. P. and Gentili, B.: Functioning of the Mediterranean Sea: past and present changes related to freshwater input and climate changes, J. Marine Syst., 20, 33–47, 1999.

Bianchi, D., Zavatarelli, M., Pinardi, N., Capozzi, R., Capotondi, L., Corselli, C., and Masina, S.: Simulations of ecosystem response during the sapropel S1 deposition event, Palaeogeogr. Palaeocl., 235, 265–287, 2006.

Blanchet, C. L., Frank, M., and Schouten, S.: Asynchronous Changes in Vegetation, Runoff and Erosion in the Nile River Watershed during the Holocene, PLoS ONE, 9, e115958, doi:10.1371/journal.pone.0115958, 2014.

Calvert, S. E. and Fontugne, M. R.: On the late Pleistocene-Holocene sapropel record of climatic and oceanographic variability in the eastern Mediterranean, Paleoceanography, 16, 78–94, 2001.

Cartapanis, O., Tachikawa, K., and Bard, E.: Northeastern Pacific oxygen minimum zone variability over the past 70 kyr: impact of biological production and oceanic ventilation, Paleoceanography, 26, PA4208, doi:10.1029/2011PA002126, 2011.

Cartapanis, O., Tachikawa, K., Romero, O. E., and Bard, E.: Persistent millennial-scale link between Greenland climate and northern Pacific Oxygen Minimum Zone under interglacial conditions, Clim. Past, 10, 405–418, doi:10.5194/cp-10-405-2014, 2014.

Casford, J. S. L., Rohling, E. J., Abu-Zied, R. H., Fontanier, C., Jorissen, F. J., Leng, M. J., Schmiedl, G., and Thomson, J.: A dynamic concept for eastern Mediterranean circulation and oxygenation during sapropel formation, Palaeogeogr. Palaeocl., 190, 103–119, 2003.

Castañeda, I. S., Schefuß, E., Pätzold, J., Sinninghe Damsté, J. S., Weldeab, S., and Schouten, S.: Millennial-scale sea surface temperature changes in the eastern Mediterranean (Nile River Delta region) over the last 27 000 years, Paleoceanography, 25, PA1208, doi:10.1029/2009PA001740, 2010.

Castradori, D.: Calcareous nannofossils and the origin of eastern Mediterranean sapropels, Paleoceanography, 8, 459–471, 1993.

Chandra, A. P. and Gerson, A. R.: Pyrite (FeS_2) oxidation: a submicron synchrotron investigation of the initial steps, Geochim. Cosmochim. Ac., 75, 6239–6254, 2011.

Cutter, G. A., Cutter, L. S., Featherstone, A. M., and Lohrenz, S. E.: Antimony and arsenic biogeochemistry in the western Atlantic Ocean, Deep-Sea Res. Pt. II, 48, 2895–2915, 2001.

De Lange, G. J., Thomson, J., Reitz, A., Slomp, C. P., Speranza Principato, M., Erba, E., and Corselli, C.: Synchronous basin-wide formation and redox-controlled preservation of a Mediterranean sapropel, Nat. Geosci., 1, 606–610, 2008.

deMenocal, P., Ortiz, J., Guilderson, T., Adkins, J., Sarnthein, M., Baker, L., and Yarusinsky, M.: Abrupt onset and termination of the African Humid Period: rapid climate responses to gradual insolation forcing, Quaternary Sci. Rev., 19, 347–361, 2000.

De Rijk, S., Hayes, A., and Rohling, E. J.: Eastern Mediterranean sapropel S1 interruption: an expression of the onset of climatic deterioration around 7 ka BP, Mar. Geol., 153, 337–343, 1999.

Emeis, K.-C., Struck, U., Schulz, H.-M., Rosenberg, R., Bernasconi, S., Erlenkeuser, H., Sakamoto, T., and Martinez-Ruiz, F.: Temperature and salinity variations of Mediterranean Sea surface waters over the last 16 000 years from records of planktonic stable oxygen isotopes and alkenone unsaturation ratios, Palaeogeogr. Palaeocl., 158, 259–280, 2000.

Emeis, K.-C., Schulz, H., Struck, U., Rossignol-Strick, M., Erlenkeuser, H., Howell, M. W., Kroon, D., Mackensen, A., Ishizuka, S., Oba, T., Sakamoto, T., and Koizumi, I.: Eastern Mediterranean surface water temperatures and $\delta^{18}O$ composition during deposition of sapropels in the late Quaternary, Paleoceanography, 18, 1005, doi:10.1029/2000PA000617, 2003.

Essallami, L., Sicre, M. A., Kallel, N., Labeyrie, L., and Siani, G.: Hydrological changes in the Mediterranean Sea over the last 30 000 years, Geochem. Geophy. Geosy., 8, Q07002, doi:10.1029/2007GC001587, 2007.

Fontugne, M. R. and Calvert, S. E.: Late Pleistocene Variability of the Carbon Isotopic Composition of Organic Matter in the Eastern Mediterranean: Monitor of Changes in Carbon Sources and Atmospheric CO Concentrations, Paleoceanography, 7, 1–20, 1992.

Grelaud, M., Marino, G., Ziveri, P., and Rohling, E. J.: Abrupt shoaling of the nutricline in response to massive freshwater flooding at the onset of the last interglacial sapropel event, Paleoceanography, 27, PA3208, doi:10.1029/2012PA002288, 2012.

Grimm, R.: Simulating the Early Holocene Eastern Mediterranean Sapropel Formation Using an Ocean Biogeochemical Model, PhD thesis, International Max Planck Research School on Earth System Modelling, Max Planck Institute, Hamburg, Germany, 2012.

Hartnett, H. E., Keil, R. G., Hedges, J. I., and Devol, A. H.: Influence of oxygen exposure time on organic carbon preservation in continental margin sediments, Nature, 391, 572–575, 1998.

Hennekam, R., Jilbert, T., Schnetger, B., and de Lange, G. J.: Solar forcing of Nile discharge and sapropel S1 formation in the early

to middle Holocene eastern Mediterranean, Paleoceanography, 29, 2013PA002553, doi:10.1002/2013PA002553, 2014.

Herut, B., Almogi-Labin, A., Jannink, N., and Gertman, I.: The seasonal dynamics of nutrient and chlorophyll *a* concentrations on the SE Mediterranean shelf-slope, Oceanol. Acta, 23, 771–782, 2000.

Jorissen, F. J.: Benthic foraminiferal successions across Late Quaternary Mediterranean sapropels, Mar. Geol., 153, 91–101, 1999.

Jorissen, F. J., de Stigter, H. C., and Widmark, J. G. V.: A conceptual model explaining benthic foraminiferal microhabitats, Mar. Micropaleontol., 26, 3–15, 1995.

Kallel, N., Paterne, M., Duplessy, J. C., Vergnaud-Grazzini, C., Pujol, C., Labeyrie, L. D., Arnold, M., Fontugne, M. R., and Pierre, C.: Enhanced rainfall in the Mediterranean region during the last sapropel event, Oceanol. Acta, 20, 697–712, 1997.

Klinkhammer, G. P. and Palmer, M. R.: Uranium in the oceans: where it goes and why, Geochim. Cosmochim. Ac., 55, 1799–1806, 1991.

Kotthoff, U., Pross, J., Müller, U. C., Peyron, O., Schmiedl, G., Schulz, H., and Bordon, A.: Climatic dynamics in the borderlands of the Aegean Sea during formation of sapropel S1 deduced from a marine pollen record, Quaternary Sci. Rev., 27, 832–845, 2008.

Krom, M. D., Michard, A., Cliff, R. A., and Strohle, K.: Sources of sediment to the Ionian Sea and western Levantine basin of the Eastern Mediterranean during S-1 sapropel times, Mar. Geol., 160, 45–61, 1999.

Kuhnt, T., Schmiedl, G., Ehrmann, W., Hamann, Y., and Hemleben, C.: Deep-sea ecosystem variability of the Aegean Sea during the past 22 kyr as revealed by Benthic Foraminifera, Mar. Micropaleontol., 64, 141–162, 2007.

Kutzbach, J. E., Chen, G., Cheng, H., Edwards, R. L., and Liu, Z.: Potential role of winter rainfall in explaining increased moisture in the Mediterranean and Middle East during periods of maximum orbitally-forced insolation seasonality, Clim. Dynam., 42, 1079–1095, 2014.

Large, R. R., Halpin, J. A., Danyushevsky, L. V., Maslennikov, V. V., Bull, S. W., Long, J. A., Gregory, D. D., Lounejeva, E., Lyons, T. W., Sack, P. J., McGoldrick, P. J., and Calver, C. R.: Trace element content of sedimentary pyrite as a new proxy for deep-time ocean–atmosphere evolution, Earth Planet. Sc. Lett., 389, 209–220, 2014.

Laskar, J., Robutel, P., Joutel, F., Gastineau, M., Correia, A. C. M., and Levrard, B.: A long-term numerical solution for the insolation quantities of the Earth, Astron. Astrophys., 428, 261–285, 2004.

Locarnini, R. A., Mishonov, A. V., Antonov, J. I., Boyer, T. P., Garcia, H. E., Baranova, O. K., Zweng, M. M., and Johnson, D. R.: World Ocean Atlas 2009, Volume 1: Temperature, in: NOAA Atlas NESDIS 68, edited by: Levitus, S., U.S. Government Printing Office, Washington, D.C., 2010.

Magny, M., Combourieu-Nebout, N., de Beaulieu, J. L., Bout-Roumazeilles, V., Colombaroli, D., Desprat, S., Francke, A., Joannin, S., Ortu, E., Peyron, O., Revel, M., Sadori, L., Siani, G., Sicre, M. A., Samartin, S., Simonneau, A., Tinner, W., Vannière, B., Wagner, B., Zanchetta, G., Anselmetti, F., Brugiapaglia, E., Chapron, E., Debret, M., Desmet, M., Didier, J., Essallami, L., Galop, D., Gilli, A., Haas, J. N., Kallel, N., Millet, L., Stock, A., Turon, J. L., and Wirth, S.: North–south palaeohydrological contrasts in the central Mediterranean during the Holocene: tentative synthesis and working hypotheses, Clim. Past, 9, 2043–2071, doi:10.5194/cp-9-2043-2013, 2013.

Marino, G., Rohling, E. J., Sangiorgi, F., Hayes, A., Casford, J. L., Lotter, A. F., Kucera, M., and Brinkhuis, H.: Early and middle Holocene in the Aegean Sea: interplay between high and low latitude climate variability, Quaternary Sci. Rev., 28, 3246–3262, 2009.

Mayewski, P. A., Meeker, L. D., Twickler, M. S., Whitlow, S., Yang, Q., Lyons, W. B., and Prentice, M.: Major features and forcing of high-latitude Northern Hemisphere atmospheric circulation using a 110 000-year-long glaciochemical series, J. Geophys. Res., 102, 26345–26366, 1997.

McLennan, S. M.: Relationships between the trace element composition of sedimentary rocks and upper continental crust, Geochem. Geophy. Geosy., 2, 1021, doi:10.1029/2000GC000109, 2001.

Meijer, P. T. and Tuenter, E.: The effect of precession-induced changes in the Mediterranean freshwater budget on circulation at shallow and intermediate depth, J. Marine Syst., 68, 349–365, 2007.

Moodley, L., Middelburg, J. J., Herman, P. M. J., Soetaert, K., and de Lange, G. J.: Oxygenation and organic-matter preservation in marine sediments: direct experimental evidence from ancient organic carbon-rich deposits, Geology, 33, 889–892, 2005.

Myers, P. G. and Rohling, E. J.: Modelling a 200-yr interruption of the Holocene Sapropel S_1, Quaternary Res., 53, 98–104, 2000.

Myers, P. G., Haines, K., and Rohling, E. J.: Modeling the paleo-circulation of the Mediterranean: the Last Glacial Maximum and the Holocene with emphasis on the formation of sapropel S1, Paleoceanography, 13, 586–606, 1998.

Nameroff, T. J., Balistrieri, L. S., and Murray, J. W.: Suboxic trace metal geochemistry in the eastern tropical North Pacific, Geochim. Cosmochim. Ac., 66, 1139–1158, 2002.

Passier, H. F., Middelburg, J. J., van Os, B. J. H., and de Lange, G. J.: Diagenetic pyritisation under eastern Mediterranean sapropels caused by downward sulphide diffusion, Geochim. Cosmochim. Ac., 60, 751–763, 1996.

Pierre, C.: The oxygen and carbon isotope distribution in the Mediterranean water masses, Mar. Geol., 153, 41–55, 1999.

Pinardi, N. and Masetti, E.: Variability of the large scale general circulation of the Mediterranean Sea from observations and modelling: a review, Palaeogeogr. Palaeocl., 158, 153–173, 2000.

Pross, J., Kotthoff, U., Müller, U. C., Peyron, O., Dormoy, I., Schmiedl, G., Kalaitzidis, S., and Smith, A. M.: Massive perturbation in terrestrial ecosystems of the Eastern Mediterranean region associated with the 8.2 kyr BP climatic event, Geology, 37, 887–890, 2009.

Reimer, P. J., Bard, E., Bayliss, A., Beck, J. W., Blackwell, P. G., Bronk Ramsey, C., Buck, C. E., Cheng, H., Edwards, R. L., Friedrich, M., Grootes, P. M., Guilderson, T. P., Haflidason, H., Hajdas, I., Hatté, C., Heaton, T. J., Hoffmann, D. L., Hogg, A. G., Hughen, K. A., Kaiser, K. F., Kromer, B., Manning, S. W., Niu, M., Reimer, R. W., Richards, D. A., Scott, E. M., Southon, J. R., Staff, R. A., Turney, C. S. M., and van der Plicht, J.: IntCal13 and Marine13 Radiocarbon Age Calibration Curves 0–50 000 Years cal BP, Radiocarbon, 55, 1869–1887, 2013.

Reitz, A., Thomson, J., de Lange, G. J., and Hensen, C.: Source and development of large manganese enrichments above east-

ern Mediterranean sapropel S1, Paleoceanography, 21, PA3007, doi:10.1029/2005PA001169, 2006.

Renssen, H., Brovkin, V., Fichefet, T., and Goosse, H.: Simulation of the Holocene climate evolution in Northern Africa: the termination of the African Humid Period, Quatern. Int., 150, 95–102, 2006.

Revel, M., Ducassou, E., Grousset, F. E., Bernasconi, S. M., Migeon, S., Revillon, S., Mascle, J., Murat, A., Zaragosi, S., and Bosch, D.: 100 000 years of African monsoon variability recorded in sediments of the Nile margin, Quaternary Sci. Rev., 29, 1342–1362, 2010.

Revel, M., Colin, C., Bernasconi, S., Combourieu-Nebout, N., Ducassou, E., Grousset, F., Rolland, Y., Migeon, S., Bosch, D., Brunet, P., Zhao, Y., and Mascle, J.: 21 000 years of Ethiopian African monsoon variability recorded in sediments of the western Nile deep-sea fan, Reg. Environ. Change, 14, 1685–1696, doi:10.1007/s10113-014-0588-x, 2014.

Roether, W., Manca, B. B., Klein, B., Bregant, D., Georgopoulos, D., Beitzei, V., Kovacevic, V., and Luchetta, A.: Recent changes in Eastern Mediterranean Deep Waters, Science, 271, 333–335, 1996.

Rohling, E. J.: Review and new aspects concerning the formation of eastern Mediterranean sapropels, Mar. Geol., 122, 1–28, 1994.

Rohling, E. J., Jorissen, F. J., and De Stigter, H. C.: 200 year interruption of Holocene sapropel formation in the Adriatic Sea, J. Micropalaeontol., 16, 97–108, 1997.

Rohling, E. J., Mayewski, P., Abu-Zied, R., Casford, J., and Hayes, A.: Holocene atmosphere–ocean interactions: records from Greenland and the Aegean Sea, Clim. Dynam., 18, 587–593, 2002.

Rohling, E. J., Marino, G., and Grant, K. M.: Mediterranean climate and oceanography, and the periodic development of anoxic events (sapropels), Earth-Sci. Rev., 143, 62–97, 2015.

Rossignol-Strick, M., Nesteroff, W., Olive, P., and Vergnaud-Grazzinni, C.: After the deluge: mediterranean stagnation and sapropel formation, Nature, 295, 105–110, 1982.

Schlitzer, R. (Ed.): Ocean Data View, available at: http://odv.awi.de, last access: September 2014, 2009.

Schmiedl, G., Kuhnt, T., Ehrmann, W., Emeis, K.-C., Hamann, Y., Kotthoff, U., Dulski, P., and Pross, J.: Climatic forcing of eastern Mediterranean deep-water formation and benthic ecosystems during the past 22 000 years, Quaternary Sci. Rev., 29, 3006–3020, 2010.

Shimmield, G. B. and Price, N. B.: The behaviour of molybdenum and manganese during early sediment diagenesis – offshore Baja California, Mexico, Mar. Chem., 19, 261–280, 1986.

Siani, G., Paterne, M., Arnold, M., Bard, E., Mativier, B., Tisnerat, N., and Bassinot, F.: Radiocarbon reservoir ages in the Mediterranean Sea and Black Sea, Radiocarbon, 42, 271–280, 2000.

Siani, G., Paterne, M., Michel, E., Sulpizio, R., Sbrana, A., Arnold, M., and Haddad, G.: Mediterranean Sea surface radiocarbon reservoir age changes since the last glacial maximum, Science, 294, 1917–1920, 2001.

Siani, G., Magny, M., Paterne, M., Debret, M., and Fontugne, M.: Paleohydrology reconstruction and Holocene climate variability in the South Adriatic Sea, Clim. Past, 9, 499–515, doi:10.5194/cp-9-499-2013, 2013.

Soulet, G., Menot, G., Lericolais, G., and Bard, E.: A revised calendar age for the last reconnection of the Black Sea to the global ocean, Quaternary Sci. Rev., 30, 1019–1026, 2011.

Stratford, K., Williams, R. G., and Myers, P. G.: Impact of the circulation on Sapropel Formation in the eastern Mediterranean, Global Biogeochem. Cy., 14, 683–695, 2000.

Stuiver, M. and Reimer, P. J.: CALIB Radiocarbon Calibration Program, available at: http://calib.qub.ac.uk/calib/, last access: September 2014, 1986–2013.

Thomson, J., Higgs, N. C., Wilson, T. R. S., Croudace, I. W., De Lange, G. J., and Van Santvoort, P. J. M.: Redistribution and geochemical behaviour of redox-sensitive elements around S1, the most recent eastern Mediterranean sapropel, Geochim. Cosmochim. Ac., 59, 3487–3501, 1995.

Thomson, J., Mercone, D., De Lange, G. J., and Van Santvoort, P. J. M.: Review of recent advances in the interpretation of eastern Mediterranean sapropel S1 from geochemical evidence, Mar. Geol., 153, 77–89, 1999.

Tjallingii, R., Röhl, U., Kolling, M., and Bickert, T.: Influence of the water content on X-ray fluorescence core-scanning measurements in soft marine sediments, Geochem. Geophy. Geosy., 8, Q02004, doi:10.1029/2006GC001393, 2007.

Tomczak, M. and Godfrey, J. S.: Regional Oceanography: an Introduction, Elsevier, Oxford, 1994.

Tribovillard, N., Algeo, T. J., Lyons, T., and Riboulleau, A.: Trace metals as paleoredox and paleoproductivity proxies: an update, Chem. Geol., 232, 12–32, 2006.

van Santvoort, P. J. M., de Lange, G. J., Thomson, J., Cussen, H., Wilson, T. R. S., Krom, M. D., and Ströhle, K.: Active post-depositional oxidation of the most recent sapropel (S1) in sediments of the eastern Mediterranean Sea, Geochim. Cosmochim. Ac., 60, 4007–4024, 1996.

Vidal, L., Menot, G., Joly, C., Bruneton, H., Rostek, F., Cagatay, M. N., Major, C., and Bard, E.: Hydrology in the Sea of Marmara during the last 23 ka: implications for timing of Black Sea connections and sapropel deposition, Paleoceanography, 25, PA1205, doi:10.1029/2009PA001735, 2010.

Waelbroeck, C., Labeyrie, L., Michel, E., Duplessy, J.-C., McManus, J. F., Lambeck, K., Balbon, E., and Labranche, M.: Sea-level and deep water temperature changes derived from benthic foraminifera isotopic records, Quaternary Sci. Rev., 21, 295–305, 2002.

Wehausen, R. and Brumsack, H.-J.: Chemical cycles in Pliocene sapropel-bearing and sapropel-barren eastern Mediterranean sediments, Palaeogeogr. Palaeocl., 158, 325–352, 2000.

Weldeab, S., Menke, V., and Schmiedl, G.: The pace of East African monsoon evolution during the Holocene, Geophys. Res. Lett., 41, 1724–1731, doi:10.1002/2014GL059361, 2014.

Ziegler, M., Jilbert, T., de Lange, G. J., Lourens, L. J., and Reichart, G.-J.: Bromine counts from XRF scanning as an estimate of the marine organic carbon content of sediment cores, Geochem. Geophy. Geosy., 9, Q05009, doi:10.1029/2007GC001932, 2008.

Ziegler, M., Tuenter, E., and Lourens, L. J.: The precession phase of the boreal summer monsoon as viewed from the eastern Mediterranean (ODP Site 968), Quaternary Sci. Rev., 29, 1481–1490, 2010.